Available online at www.sciencedirect.com
ScienceDirect
Earth and Planetary Science Letters 263 (2007) 180–191
EPSL
www.elsevier.com/locate/epsl

Evidence of former stishovite in metamorphosed sediments, implying subduction to >350 km

Liang Liu [a,b], Junfeng Zhang [b,d], Harry W. Green II [b,c,*], Zhenmin Jin [d], Krassmir N. Bozhilov [b]

[a] State Key Laboratory of Continental Dynamics, Department of Geology, Northwest University, Xi'an 710069, China
[b] Institute of Geophysics and Planetary Physics, University of California, Riverside, CA 92521, USA
[c] Department of Earth Sciences, University of California, Riverside, CA 92521, USA
[d] State Key Laboratory of Geological Processes and Mineral Resources, China University of Geosciences, Wuhan 430074, China

Received 8 May 2007; received in revised form 14 July 2007; accepted 11 August 2007
Available online 23 August 2007
Editor: G.D. Price

Abstract

Deep subduction of continental rocks or sediments has until recently been considered impossible because they are buoyant relative to mantle compositions. Nevertheless, it has been shown over the last 20 yr that during continental collision, such rocks can be subducted to >200 km and returned to the surface. Delineation of the depth to which continental materials can be subducted is important for understanding continental collision processes and interpretation of the geochemical signals in mantle magmas. Here we report oriented aluminum- and iron-bearing oxide inclusions in quartz of "ultra-high-pressure" rocks from the Altyn Tagh, western China, already known to have seen depths of more than 200 km. Laboratory experiments at high pressure show that inclusion abundances are not consistent with precipitation from quartz or coesite but are consistent with precipitation from stishovite (SiO_2 polymorph stable only above ~9 GPa pressure). Further, geometrical relationships between the oriented inclusions demonstrate that the original host mineral must have had tetragonal symmetry and lattice spacings consistent with those of stishovite. The sum of these data establish that sediments can be subducted to at least 350 km and returned to the surface, a depth close to the "point of no return" where continental materials would have density comparable to the mantle and would "fall" to at least the base of the mantle transition zone where they could contribute to the continental trace element "signal" in ocean island basalts.

Keywords: ultra-high-pressure metamorphism; continental collision; precipitate; topotaxy; mantle transition zone

1. Introduction

"Ultra-high-pressure metamorphism" (UHPM), stimulated by discovery of coesite (Chopin, 1984; Smith, 1984) and microdiamonds (Sobolev and Shatsky, 1990) in continental collision terranes has been one of the most rapidly moving fields in geology over the last two decades. During this time, evidence has accumulated that during continental collision, sediments and "granitic" rocks, despite their inherent buoyancy, have been subducted to >200 km and returned to the surface (Ye et al., 2000; Ogasawara et al., 2002; Zhang et al., 2005). Evidence based on mineral exsolution (precipitation)

* Corresponding author. Department of Earth Sciences, University of California, Riverside, CA 92521, USA. Tel.: +1 951 8274505; fax: +1 951 8274324.
E-mail address: harry.green@ucr.edu (H.W. Green).

0012-821X/$ - see front matter © 2007 Elsevier B.V. All rights reserved.
doi:10.1016/j.epsl.2007.08.010

microstructures has shown that mantle rocks can be exhumed to the surface from even greater depths (Dobrzhinetskaya et al., 1996; Van Roermund and Drury, 1998; Bozhilov et al., 1999; Liu et al., 2007), raising questions as to whether continental rocks can be subducted to such depths that they become more dense than the ambient mantle (Irifune et al., 1994) and therefore cannot be returned to the surface.

With increasing pressure, quartz, one of the major minerals of continental crust, transforms sequentially into its high-pressure polymorphs coesite (~3 GPa) and stishovite (9–10 GPa), corresponding to about 100 and 300 km respectively (Chopin, 1984; Ono, 1998). Although coesite is well-documented in ultra-high-pressure metamorphic terranes and mantle xenoliths (Smyth and Hatton, 1977; Ogasawara et al., 2002; Zhang et al., 2005), stishovite has been reported only in meteorites and impact craters (Chao et al., 1962; Sharp et al., 1999; El Goresy et al., 2000).

Experiments show that a few weight percent Al_2O_3 can dissolve into stishovite (Irifune and Ringwood, 1993; Pawley et al., 1993) and therefore it is expected that similar Al_2O_3-bearing stishovite exists in deeply subducted mid-ocean ridge basalt at pressures greater than 9 GPa (Irifune et al., 1994; Ono, 1998; Chung and Kagi, 2002). In contrast, less than 0.2 wt.% Al_2O_3 has been reported from natural or experimental coesite and quartz (Smyth and Hatton, 1977; Irifune et al., 1994; Ono, 1998; Landtwing and Pettke, 2005). It is therefore predicted that SiO_2-rich rocks subducted to more than 300 km should develop stishovite with significant dissolved Al_2O_3 and that subsequent exhumation would induce exsolution of Al-rich phase(s) before and/or during transformation to coesite.

2. Materials and methods

The rock reported here is a pelitic gneiss composed of garnet (20–25 vol.%), kyanite (25–30%), perthite (30–35%) and quartz (10–15%), with minor retrograde biotite, plagioclase and sillimanite. For high-pressure experiments to investigate the solubility of Al and Fe in SiO_2, materials were fabricated as follows: Gem quality crystals of almandine, kyanite, quartz and microcline were crushed separately to small particles and ground into very fine (<5 μm) powders in alcohol. During crushing, powders were examined carefully under the optical microscope and impurities were removed by hand. Two starting materials were prepared: (i) 30 wt.% almandine, 20 wt.% kyanite, 15 wt.% microcline, 32 wt.% quartz and 3 wt.% H_2SiO_3 (to enhance reaction kinetics); (ii) an identical mixture but with 5 wt.% hematite powder added (Table 1).

Specimen assemblies of semi-sintered MgO octahedra (Aremco Products #584-OS) were used, with a cylindrical heater of two rolls of 0.0254 mm thick Re-foil. Pressure calibration of the apparatus was performed at room temperature (Green et al., 2000) and at high temperature using the coesite/stishovite boundary. Starting powders were loaded into a platinum capsule 4.0 mm long and 2.5 mm in diameter. A disc of Ni foil was placed at one end of the capsule of Fe_2O_3-free experiments, to buffer fO_2. In the Fe_2O_3-bearing system, fO_2 was controlled by excess hematite. Temperature was monitored by a single W/Re thermocouple (uncorrected for pressure) located ~1 mm below the furnace midpoint. For this assembly, the temperature is about 80 °C less at the ends of the capsule than at its center (Dobrzhinetskaya et al., 2004). Samples were pressurized to the desired pressure in a Walker-style multianvil apparatus (Rockland Research) using 6 mm truncated edge WC cubes, heated at a rate of 20 °C/min, held at a constant temperature (normally for 24 h), quenched by turning off the power, and slowly depressurized. Recovered samples were split longitudinally and prepared as polished sections for optical and electron microscopy.

We conducted both single-stage experiments (in which samples were simply pressurized, heated, annealed, and quenched) and two-stage experiments in which specimens were subjected to conditions similar to the first type and then annealed for a second period at lower pressure and/or temperature (Table 2). The former

Table 1
Chemical compositions of natural samples and experimental starting materials

Material	SiO_2	TiO_2	Al_2O_3	Fe_2O_3	FeO	MgO	MnO	CaO	Na_2O	K_2O	H_2O	Total
Natural sample	48.69	0.97	31.27	2.58	6.06	2.79	0.09	0.40	0.65	5.52		99.91
Fe_2O_3-free system [a]	59.34	0.00	26.51	0.00	7.59	1.47	0.28	0.48	1.02	2.63	0.69	100.00
Fe_2O_3-bearing system [b]	56.52	0.00	25.25	4.76	7.23	1.40	0.27	0.45	0.97	2.50	0.66	100.00

[a] This composition consists of 30 wt.% garnet (Alm, 68.3%; Prp, 23.6%; Grs, 5.5%; Sps, 2.6%), 20 wt.% kyanite, 32 wt.% quartz, 15 wt.% microcline (Or, 62.8%; Ab, 37.2%) and 3 wt.% H_2SiO_3.

[b] This composition consists of 28.6 wt.% garnet (Alm, 68.3%; Prp, 23.6%; Grs, 5.5%; Sps, 2.6%), 19.1 wt.% kyanite, 30.5 wt.% quartz, 14.3 wt.% microcline (Or, 62.8%; Ab, 37.2%), 2.9 wt.% H_2SiO_3 and 4.8 wt.% Fe_2O_3.

Table 2
Chemical compositions of stishovite and coesite in run products and experimental results

	SiO_2	Al_2O_3	Fe_2O_3[a]	MgO	CaO	MnO	Na_2O	K_2O	Total[b]	Si	Al	Fe	Al+Fe	Experimental results					
														P (GPa)	*T* (°C)	*t* (h)	Products	Starting materials	Run#
St	97.23	1.34	0.69	0.04	0.00	0.01	0.00	0.01	99.32	0.978	0.016	0.005	0.021	11	1400	19	Gt,Ky,St,Ho	2[c]	MA249
St	97.35	1.17	0.56	0.02	0.00	0.01	0.01	0.00	99.12	0.980	0.014	0.004	0.018	10	1300	29	Gt,Ky,St,Ho	2	MA250
St	98.54	0.43	0.28	0.01	0.00	0.00	0.01	0.00	99.27	0.990	0.005	0.002	0.007	10	1000	29	Gt,Ky,St,Ho	2	MA281
Coe	98.52	0.11	0.03	0.00	0.00	0.00	0.00	0.00	98.67	0.997	0.002	0.000	0.002	8	1300	20	Gt,Ky,Coe,Kf	2	MA252
St	98.58	1.22	0.01	0.02	0.00	0.00	0.01	0.00	99.84	0.989	0.014	0.000	0.014	12	1200	24	Gt,Ky,St,Ho	1[d]	MA252
St	97.96	1.66	0.03	0.03	0.00	0.01	0.00	0.00	99.80	0.978	0.021	0.000	0.021	12	1400	25	Gt,Ky,St,Ho	1	MA247
St	97.62	1.64	0.03	0.04	0.00	0.01	0.01	0.00	99.34	0.990	0.020	0.000	0.020	11	1400	18	Gt,Ky,St,Ho	1	MA248
St	97.44	1.59	0.03	0.03	0.00	0.01	0.00	0.00	99.10	0.980	0.019	0.000	0.019	10	1450[e]	24	Gt,Ky,St(coe),Ho	1	MA244
Coe	98.88	0.10	0.02	0.01	0.00	0.00	0.01	0.00	99.02	0.998	0.001	0.000	0.001						
Coe	99.35	0.12	0.03	0.00	0.00	0.00	0.00	0.00	99.50	0.998	0.002	0.000	0.002	8	1200	25	Gt,Ky,Coe,Kf	1	MA242
Coe	99.43	0.14	0.03	0.00	0.00	0.01	0.00	0.00	99.60	0.998	0.002	0.000	0.002	6	1200	24	Gt,Ky,Coe,Kf	1	MA246
St	98.46	0.83	0.22	0.02	0.01	0.00	0.01	0.00	99.53	0.988	0.010	0.002	0.012	11	1400	18.5	Gt,Ky,St	3[g]	MA265[f]
														11	1200	24			
St	98.42	0.82	0.26	0.02	0.00	0.00	0.01	0.00	99.54	0.987	0.010	0.002	0.012	11	1400	20	Gt,Ky,St,Ho	2	MA269[f]
														11	1200	24			
St	98.21	0.80	0.22	0.01	0.00	0.00	0.00	0.01	99.25	0.988	0.009	0.002	0.011	11	1400	14	Gt,Ky,St,Ho	2	MA269[f]
														9	1200	5			
St	98.17	0.25	0.21	0.02	0.01	0.00	0.01	0.00	98.67	0.995	0.003	0.002	0.005	11	1300	22	Gt,Ky,St,Ho	2	MA277[f]
														9	900	23			
St	98.22	0.63	0.17	0.00	0.00	0.00	0.00	0.00	99.02	0.991	0.008	0.001	0.009	11	1300	12	Gt,Ky,St,Ho	2	MA289[f]
														9	900	2			
St	98.92	0.60	0.24	0.03	0.00	0.01	0.00	0.00	99.80	0.990	0.007	0.002	0.009	11	1350	21	Gt,Ky,St,Ho	2	MA289[f]
														9	800	12			
St	98.23	0.64	0.22	0.02	0.01	0.00	0.00	0.00	99.12	0.990	0.008	0.002	0.010	11	1300	22	Gt,Ky,St,Ho	2	MA276[f]
														9	1100	5.5			
Coe	99.61	0.00	0.03	0.00	0.00	0.01	0.01	0.00	99.65	0.999	0.000	0.000	0.000	10	1300	20	Gt,Ky,Coe,Kf	2	MA271[f]
														8	1280	5			
Coe	99.29	0.03	0.03	0.00	0.00	0.01	0.00	0.00	99.36	0.999	0.000	0.000	0.000	10	1300	20	Gt,Ky,Coe,Kf	2	MA273[f]
														8	1200	1			

a. Fe_2O_3 contents are calculated from FeO contents in the stishovite or coesite; b. TiO_2, Cr_2O_3 and NiO were also analysed for but not detected. c. Fe_2O_3-bearing system; d. Fe_2O_3-free system; e. Experiment MA244 was annealed at $P=10$ GPa and $T=1200$ °C for approximately 24 h before its heater failed. The recovered sample shows a molten platinum capsule near the thermocouple. Coesite was found to exist near the thermocouple end while stishovite was found on the other end, suggesting a high instantaneous temperature (>2100 °C) near the thermocouple and a huge thermal gradient along the specimen. Therefore, we analysed only the run products near the transformation boundary and estimate the temperature to be about 1450 °C (the temperature for stishovite/coesite phase transformation at 10 GPa). f. no microcline in starting materials; g. two-step decompression experiments. St: stishovite; Coe: coesite; *P*: pressure; *T*: temperature; *t*: duration time; Gt: garnet; Ky: kyanite; Ho: hollandite; Kf: k-feldspar.

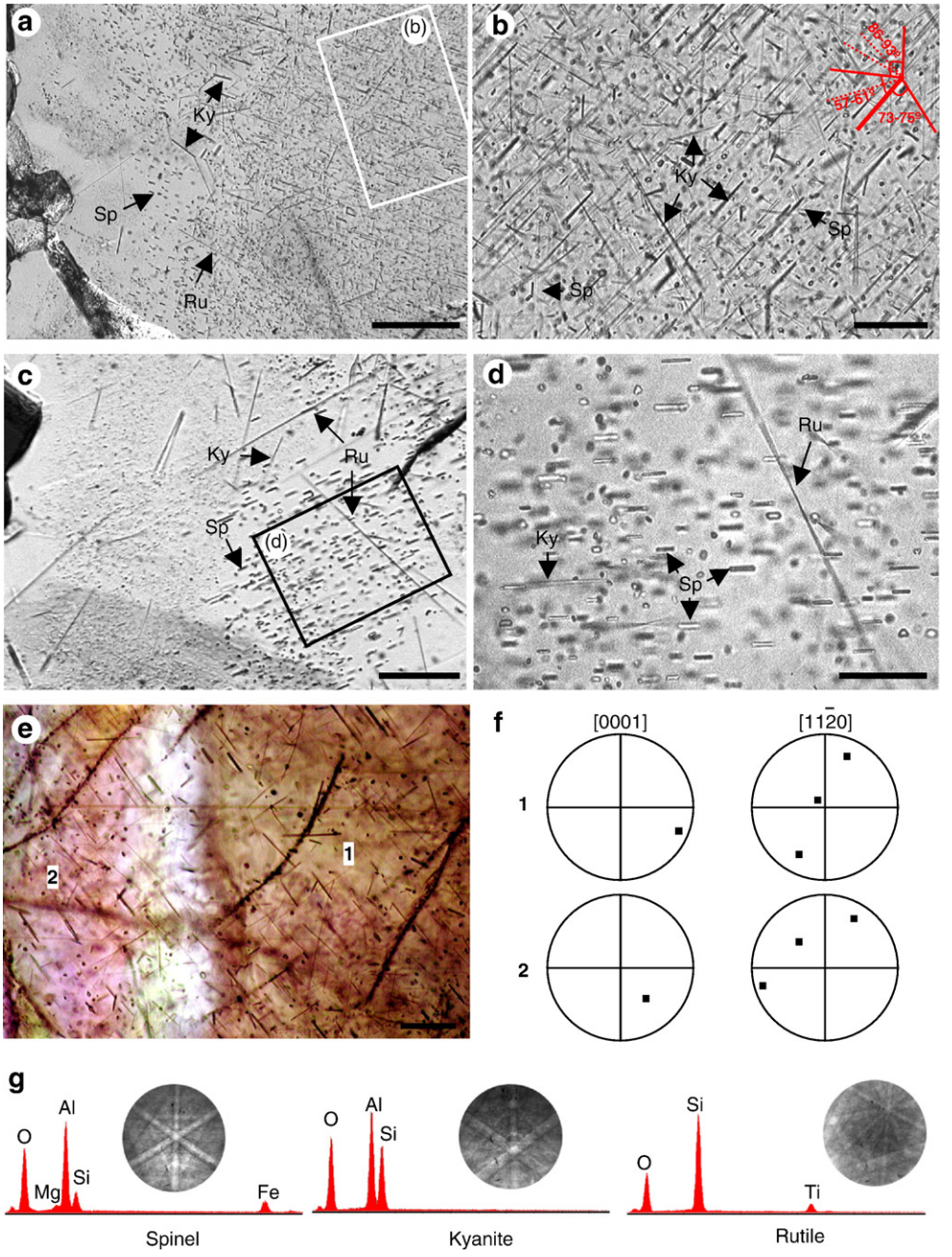

Fig. 1. Spinel, kyanite and rutile rods and needles in quartz. (a, c) Low-magnification optical transmission images showing dense concentrations of rods and needles of spinel, kyanite and rutile. Note that the left edges of both panels (adjacent to other phases) have fewer and smaller inclusions. (b, d) Detail of images (a) and (c), respectively, showing that oriented kyanite needles and spinel rods have several groups of orientations. (e) Representative pair of quartz grains (transmitted light image with crossed polarizers) showing parallel oriented rods and needles crossing a high angle (63.5°) grain boundary, implying an inherited exsolution microstructure from a pre-existing phase. Bright band marks inclined boundary between crystals. (f) Crystallographic orientations of quartz grains imaged in (e) measured by electron back-scattered diffraction (EBSD). (g) Energy-dispersive (EDS) X-ray analyses (parts of O peaks and parts or all of Si peaks are from the enclosing quartz) and EBSD patterns of spinel rods, kyanite needles and rutile needles. Note that spinel contains a small fraction of Mg (Mg:Fe ~ 1:3). Sp: hercynitic spinel; Ky: kyanite; Ru: rutile. Scale bars: a, c 200 μm; b, d 50 μm; e, 100 μm.

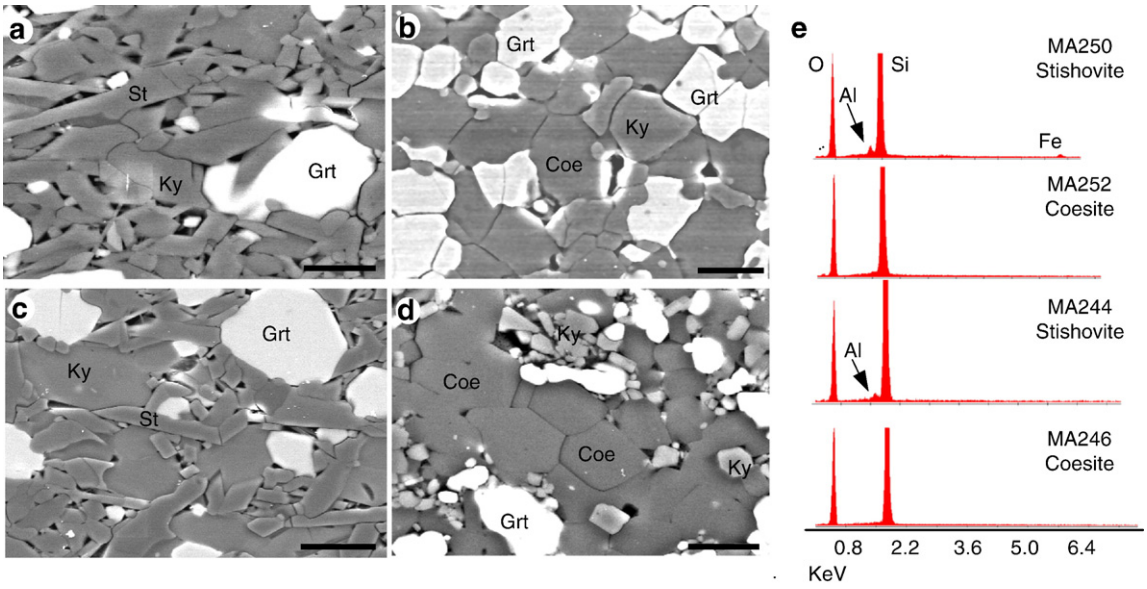

Fig. 2. Microstructures of experimental products showing grain sizes and equilibrium textures. Fe_2O_3-bearing system: (a) MA250 (10 GPa, 1300 °C); (b) MA252 (8 GPa, 1300 °C). Fe_2O_3-free system: (c) MA244 (10 GPa, 1450 °C); (d) MA246 (6 GPa, 1200 °C). All images are secondary electron SEM micrographs. (e) Energy-dispersive X-ray analyses of stishovite and coesite. A pronounced Al peak shows in stishovite but not in coesite. Fe peak shows only in stishovite of the Fe_2O_3-bearing system. St: stishovite; Ky: kyanite; Grt: garnet; Coe: coesite. Scale bars: 10 μm.

approached equilibrium from conditions of low Al and/or Fe solubility and the latter approached equilibrium from conditions of higher Al/Fe contents. To minimize the effects of thermal gradients, we analysed the run products only near the thermocouple, except for Run MA244 (see note in Table 2).

Run products were examined at UC Riverside with a Philips XL30-FEG SEM and Philips CM30 TEM, both equipped with EDAX energy dispersive X-ray microanalysis (EDS). The instruments are equipped with ultrathin window Si (Li) detectors, and a resolution of 137 eV at MnKα. Imaging of run products in the SEM was with both secondary and back-scattered electron modes at 15 and 20 keV; phases and their orientations were identified by electron back-scatter diffraction (EBSD). The chemical compositions of run products were examined with a Camebax SX51 microprobe analyser at the Institute of Geology and Geophysics, Chinese Academy of Sciences (Beijing): accelerating voltage 15 keV, beam current 20 nA, beam diameter 1 μm, counting time 10 s, PAP program for matrix correction.

3. Results

We report here observation of significant concentrations (up to ~1.5 vol.%) of kyanite, Al_2SiO_5, plus hercynitic spinel, $(Fe_{0.75},Mg_{0.25})(Al, Fe)_2O_4$, with exsolution morphology within quartz of a garnet-kyanite (pelitic) gneiss associated with eclogite at Jianggalesayi creek of the Altyn Tagh mountains of NW China. This terrane is considered the western extension of the north Qaidam Mountains UHPM terrane (Yang et al., 2002; Liu et al., 2005); both are located within the collision zone between the early

Fig. 3. Stereographic projection of kyanite/spinel orientations in two widely separated quartz domains; implications for the precursor SiO_2 phase. (a–d) crystal 1; (e, f) crystal 2. (a) Raw data for quartz domain #1 measured on a universal stage showing 7 tight orientation groups. Note that all measurements lie at less than 30° to the plane of the thin section; steeper orientations are present but cannot be measured accurately. (b) Orientation groups replaced by idealized symbols; group 1 is much more abundant than other orientations (many more needles than actually plotted), hence if the original phase was stishovite, this group must represent [001], the only unique direction in stishovite (see extended discussion in Appendix A). Orientation groups 2/3 and 6/7 define a mirror plane passing through [001]. (c) Stishovite has point-group symmetry 4/m 2/m 2/m; inserting the additional mirrors implied by this symmetry shows that one of them goes through groups 2 and 3, two others go through groups 6 and 7, respectively, and the last passes between groups 4 and 5, hence all 7 needle groups are consistent with stishovite symmetry. (d) Adding all of the other needle groups implied by the additional mirrors shows that they all lie at angles greater than 30° to the thin section and are inaccessible to measurement. Crystallographic orientations implied for stishovite are labeled in terms of the <100> axes shown. (e) Orientation groups of quartz domain #2, showing 9 different groups. (f) Construction of the mirror planes consistent with the data reveals exactly the same seven groups as in (d), plus an additional set of the symmetrical equivalents to groups 4 and 5 that appear outside the central 60° circle. See Appendix A for further discussion.

Palaeozoic Tarim-Qilian block and the Precambrian Qaidam craton but are separated by 400 km along the Altyn strike–slip fault.

The quartz of this rock is curiously distributed; it occurs only in monomineralic polycrystalline domains with dimensions ~7 mm×3 mm. Within these domains, individual quartz crystals (~0.5 mm diameter) exhibit irregular grain boundaries and contain abundant oriented needles of kyanite and rods of spinel, as well as trace amounts of rutile needles (Fig. 1). The boundaries of these quartz domains against other minerals of the rock are relatively free of inclusions (Fig. 1a and c), with their interiors densely populated with several intermixed oriented sets of kyanite needles (20−100 μm long; 0.2−0.5 μm diameter) and spinel rods (10−50 μm long; 1−2 μm diameter), a microstructure strongly suggestive of

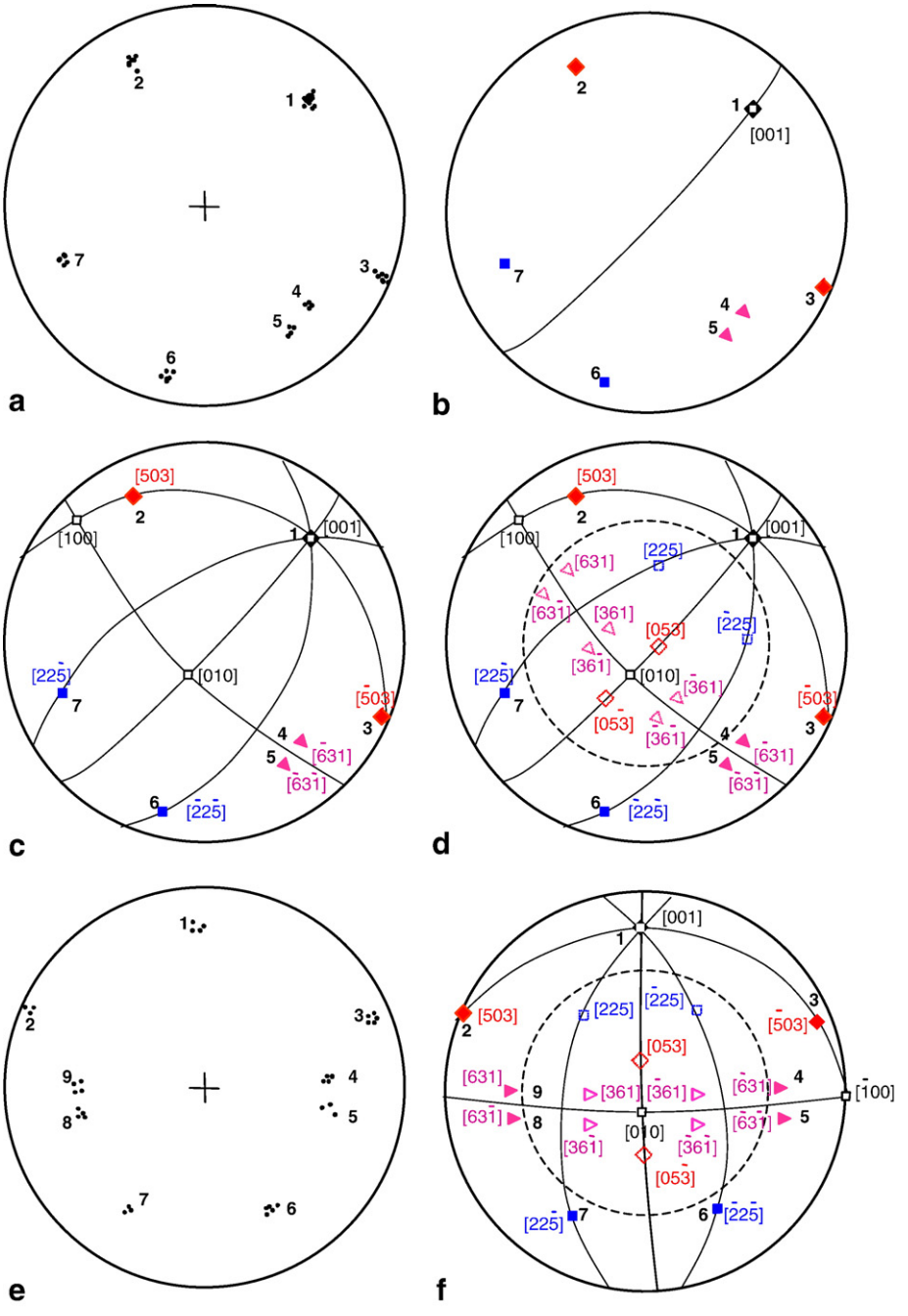

exsolution of these Al-rich phases (Fig. 1b and d). Rutile needles have apparently random orientations.

Within the quartz domains, the oriented rods and needles of kyanite and spinel remain abundant right up to and across high angle quartz boundaries with their parallelism undisturbed (Fig. 1e and f), demonstrating that they do not exhibit topotaxy with the quartz and suggesting that they originated by exsolution from a pre-existing phase of larger grain size. Fig. 1g shows the energy dispersive X-ray spectra (EDS) of the three included minerals accompanied by electron back-scattered diffraction (EBSD) patterns showing their crystallographic structures and orientations. Kyanite is elongated parallel to [001] and spinel is elongated along a <110> direction. These observations were confirmed with transmission electron microscopy (TEM). The restriction of spinel (cubic symmetry) to this rod-shaped habit requires explanation, the simplest of which is that it formed by precipitation from some pre-existing phase that constrained both its orientations and its crystallographically-controlled asymmetric shape.

We estimate volume percentage of precipitates is ~1 %, based on digital image analysis of dozens of grains from 4 polished sections viewed in both reflected light and SEM (BSE mode). The volume ratio of kyanite to spinel is ~2:1 based on both SEM and TEM observations. These estimates correspond to an original solubility of ~1.15 wt.% Al_2O_3, 0.2–0.3 wt.% FeO and 0.03–0.05 wt.% MgO in the pre-existing SiO_2 phase. Similar Al and Fe concentrations were confirmed by large-area energy-dispersive X-ray analysis [0.78–1.23 wt.% Al_2O_3 and 0.18–0.47 wt.% FeO].

It is well known that quartz accepts only very small amounts of Al or Fe into solid solution. Moreover, our microstructural observations show that the included crystals, despite having morphology indicating exsolution, have no topotactic relationship to the quartz (Fig. 1c and d). Therefore, we investigated the solubility of Al and Fe in coesite and stishovite using experimental charges similar to the natural rock (Table 1). Table 2 provides experimental conditions, times, and compositions of run products. The following observations suggest that most experiments closely approached equilibrium (Fig. 2; Table 2): (i) The grain size of new crystals (10–20 μm) in run products is generally much larger than those of the starting materials; (ii) The run products are quite homogeneous and are different minerals from the starting mix; (iii) Most samples typically show straight and flat grain boundaries with well-formed triple junctions; (iv) Al and Fe concentrations were closely bracketed by approach to equilibrium from excess and deficient compositions.

The chemical compositions of synthesized coesite and stishovite (Table 2) reveal that: (i) The Al_2O_3 solubility in coesite (0.10–0.14 wt.%) is much less than that in stishovite (0.88–1.66 wt.%); (ii) Fe was incorporated into stishovite in significant amounts only in Fe_2O_3-bearing assemblies; (iii) The solubility of Al_2O_3 in stishovite is much more than that of Fe_2O_3, with Al:Fe ~3:1; (iv) The solubility of Al_2O_3 tends to increase with both pressure and temperature.

The 5–15-fold higher concentration of Al_2O_3 in stishovite compared to coesite (Table 2) is consistent with previous studies on stishovite and coesite at high pressure (Irifune et al., 1994; Ono, 1998; Chung and Kagi, 2002). We also confirm that less than 0.1 wt.% divalent cations (Mg^{2+}, Fe^{2+}, Mn^{2+}, Ca^{2+}) are soluble in stishovite in Fe_2O_3-free systems at pressures less than 17.5 GPa (Irifune et al., 1994; Chung and Kagi, 2002). In contrast, our results show that in the Fe_2O_3-bearing system stishovite can incorporate measurable amounts of iron, (~0.6 wt.% Fe_2O_3). An earlier Mössbauer spectroscopy study demonstrated Fe^{3+} incorporation into rutile, which is isostructural with stishovite (Bromily et al., 2004). In Fe-bearing experiments, the Al concentration was generally reduced compared to Fe-free experiments, suggesting that Al^{3+} and Fe^{3+} compete for the same sites in the stishovite structure; the ratio of solubility of Al^{3+} to that of Fe^{3+} in stishovite is approximately 3:1, a result in good agreement with our natural observations. Our experimental results also show that the solubility of Al_2O_3 in stishovite increases with temperature and pressure as suggested by previous work (Ono, 1999). It is clear, therefore, that the strong microstructural implication of exsolution origin for the kyanite and spinel inclusions and the experimental solubility measurements are both inconsistent with an origin within quartz or coesite but consistent with stishovite.

To test this implication further, we measured the 3-dimensional orientation of large numbers of precipitates within 40 quartz domains (10 from each of 4 thin sections), using a universal stage. We found 7–10 tightly-constrained orientation groups in all 40 of these domains; in most cases, one orientation group was much more abundant than the others (Fig. 1b; Table A1 in the Appendix). Needle orientation measurements were restricted to less than ~30° to the plane of the thin section because at steeper angles their orientations could not be measured accurately. Both kyanite and spinel orientations may participate in all orientation groups, although it is possible that some are exclusively one phase or the other because many needles are too small to identify. In particular, both phases are abundantly present in the most common orientation (e.g., NE–SW in

Fig. 1b). Symmetry constraints require that if these precipitates formed in stishovite, the unique dominant orientation group must be parallel to [001], the only unique direction in stishovite. The family of other directions must also be consistent with the point-group symmetry of stishovite (4/m 2/m 2/m). Fig. 3 shows the patterns for two quartz domains chosen from different thin sections. In Fig. 3a, seven orientation groups are visible; Fig. 3b–d show how identification of the most abundant group as [001] and using the mirror planes present in the data lead to demonstration of tetragonal symmetry. Fig. 3e and f show that in the second quartz domain the same 7 groups are present, plus an additional pair of symmetrical equivalents of groups 4 and 5 (groups 8 and 9) appear because they are inclined at a lower angle to the thin section than in the first quartz domain. Thus, the tetragonal symmetry of the original host is firmly established, once again being consistent with stishovite and ruling out coesite or quartz. Furthermore, quantitative comparison of the [001] structure of kyanite and the [110] structure of spinel with the implied directions in stishovite (see Appendix A) reveals that the implied topotaxy between hypothetical host and precipitates is an excellent fit, further strengthening the implication of stishovite as the original SiO_2 phase.

4. Discussion

Previously proposed charge-balanced substitutions in stishovite are $M^{3+}+H^{+}=Si^{4+}$ or $2Si=2M^{3+}+O_v$ (where M^{3+} indicates Al^{3+} and/or Fe^{3+} and O_v signifies an oxygen vacancy) (Irifune and Ringwood, 1993; Pawley et al., 1993). However, the reported extremely high ratio of Al^{3+} to H^{+} solubility in stishovite indicates that the latter reaction dominates (Irifune and Ringwood, 1993; Irifune et al., 1994). Therefore, Al^{3+}- and Fe^{3+}-bearing stishovite solid solutions may be described as $(Si_{1-2x}, M^{3+}{}_{2x})O_{2-x}$ if one neglects the trace amount (normally less than 0.1 wt.%) of potential protons. Given these and our experimental results and ignoring the small Mg content of the spinel, the following exsolution reaction can be conceived within an Al^{3+}- and Fe^{3+}-bearing stishovite.

$$\begin{aligned}(Si_{1-2x}Al^{3+}_{2x-y}Fe^{3+}_{y})O_{2-x} = {} & (1-3x+3y/2)SiO_2 \\ & +(x-3y/2)Al_2SiO_5 \\ & +yFeAl_2O_4+y/4O_2\end{aligned}$$

$$\begin{aligned}&(Al-Fe^{3+}-\text{ bearing stishovite}) \\ &\quad =(\text{stishovite})+(\text{kyanite})+(\text{spinel}) \qquad (1)\end{aligned}$$

Subsequently, coesite and quartz would form sequentially at lower pressure, inheriting the exsolved minerals, as shown in Fig. 1e (Cahn, 1977).

However, examination of the literature shows that at very high pressure in this system, the equilibrium spinel composition is a solid solution between magnetite and Fe-rich ringwoodite (Woodland and O'Neill, 1993; Woodland and Angel, 2000). During decompression, the spinel structure is preserved but its composition progressively evolves toward magnetite until the pressure is below ~2 GPa, at which point, a hercynitic component becomes stable (Woodland and O'Neill, 1993) and the observed spinel composition will be established (see Appendix B for extended discussion).

This precipitation and exhumation scenario is consistent with all experimental data and natural observations. Any scenario that eliminates Al_2O_3- and Fe_2O_3-bearing stishovite as a primary phase cannot explain the abundance of precipitates, their chemistry, their orientations, their ignoring of quartz grain boundaries, or the coexistence of $(Fe_{0.75},Mg_{0.25})Al_2O_4$ spinel with kyanite. In addition to the conditions for formation of spinel with this composition, another constraint on the exhumation path is that outside of the SiO_2 domains kyanite is partially replaced by sillimanite.

Combining all of the data presented here, we arrive at a family of possible conditions of origin and exhumation paths for these rocks (Fig. 4). The reconstructed Al–Fe-bearing stishovite had ~1.15 wt.% Al_2O_3 and 0.2–0.3 wt.% Fe_2O_3 (Al+Fe=0.0153–0.0159), close to those synthesized at pressures above 10 GPa in our experiments (Table 2). Using the temperature- and pressure-dependence of solubility of Al_2O_3 in stishovite from our experiments, we conclude that exsolution of the observed amounts of precipitates within the stishovite stability field requires original pressures of 12–14 GPa, depending on the temperature at which the exhumation path left the stishovite stability field (Fig. 4). Thus, we conclude that the Altyn Tagh pelitic gneiss was metamorphosed at a minimum pressure of ~12 GPa, suggesting subduction to and exhumation from depths of 350 km or more.

This conclusion has important implications. These rocks must have been subducted very close to their "point of no return"; the stable mineralogy of average continental material at 350 km would have a density of 3.7–3.9 g cm^{-3} (Irifune et al., 1994), hence buoyancy forces would be effectively cancelled. In that case, entrainment by the sinking slab should become the predominant influence until ~660 km, the base of the mantle transition zone (Irifune et al., 1994), where such

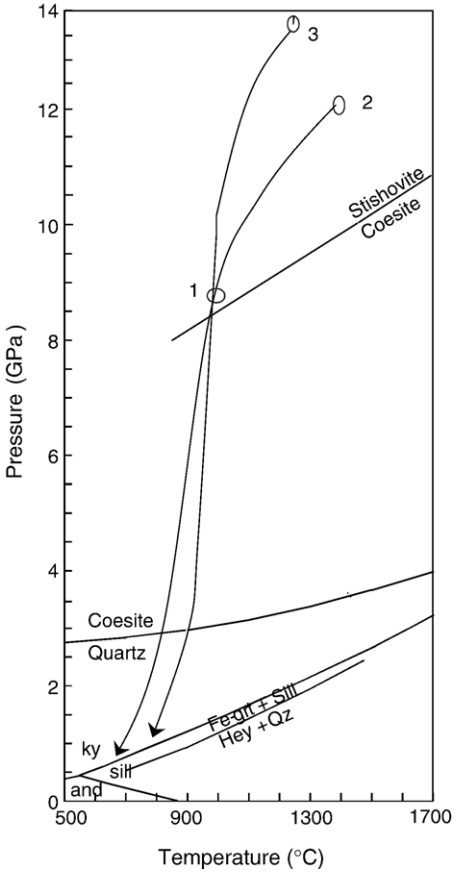

Fig. 4. Possible exhumation paths for Altyn Tagh pelitic gneiss. There are only two constraints on the P/T path followed by these rocks from the stishovite field to the surface. Firstly, the rock must have originated sufficiently far above the phase boundary to allow precipitation of the observed amounts of kyanite and spinel. An origin at point 1 or other points close to the phase boundary would not provide sufficient differences in Al- and Fe-solubility. Based on our observed temperature- and pressure-dependence of Al_2O_3 solubility in stishovite and the arbitrary assumption that the exhumation path crossed the phase boundary to coesite at ~8.5 GPa, we have plotted two potential conditions of origin that satisfy this constraint (points 2 and 3). The much higher temperature-dependence of solubility compared to the pressure-dependence allows choice of a lower pressure origin if a higher temperature is assumed. The only additional constraint on the exhumation path is that outside of the quartz domains sillimanite is found. We thus require both of the suggested exhumation paths to enter the sillimanite stability field at shallow depth. All phase transformation curves are calculations from the THERMOCALC program (Holland and Powell, 1998) with mineral thermodynamic data. These curves are in good agreement with the experimental data. See Appendix B for discussion of low pressure reactions.

rocks may play a role in the geochemical evolution of the crust–mantle system — such as source of alkali intraplate hotspot magmas (Van der Hilst et al., 1997; Sobolev et al., 2005) or kimberlites. Demonstration here that such depths can be reached by continental material also provides the basis for interpretation of inclusions in diamonds that are incompatible with expected mantle petrology, such as the recent discovery of phase egg (Wirth et al., 2007).

Acknowledgements

We thank L. Dobrzhinetskaya for helpful discussions and experimental advice. We also thank S. Gao, Y. Sun, D. Chen, J. Yang, and X. Ou for helpful discussions and collaboration in the field work, F. Forgit for technical support and apparatus maintenance, and Q. Mao, G. Shu for electron microprobe analyses. We also thank Michael Brown and several anonymous reviewers for comments that led to strengthening and clarification of the ms. This research was supported by the Natural Science Foundation of China (Grant No.40572111, 40372088, 40472043, 40502021), the Chinese Ministry of Science and Technology (Grant No. 1999075508), the Ministry of Education of China (Grant No. B07039, IRT0441, 306021), and the US National Science Foundation (Grant No. EAR0408505).

Appendix A. Precipitate orientations and topotaxy with stishovite

Based on the high-pressure, high-temperature crystallographic parameters of stishovite, kyanite, and ringwoodite/magnetite solid solution with a molar ratio of ~1:2 ($ring_{0.36}/mag_{0.64}$), and the elongation directions of spinel and kyanite rods and needles (Table A1), we deciphered the crystallographic orientation in stishovite of all 9 exsolution orientation families shown in Fig. 3 of the main text. Symmetry constraints require that if the exsolution took place from stishovite, the orientation group that is greatly in excess of all others (Group 1) would have to be parallel to the stishovite [001] axis direction because that is the only unique direction in a tetragonal lattice. No other assumptions were made; all of the remaining symmetrical and structural fits follow directly from the observations as described in the main text. There are two additional observations which strongly support these fits: (1) The structures of all three of the minerals in question here (stishovite, kyanite, spinel) have edge-sharing chains of coordination octahedra (SiO_6 and/or AlO_6); the chains lie along the [001] direction of stishovite and kyanite, and along the <110> directions of spinel. It is exactly these orientations that are shared in the most prominent orientation of kyanite and spinel needles along stishovite [001]. Thus, for this most abundant orientation, these chains are preserved during exsolution, making the interfaces between stishovite/

kyanite and stishovite/spinel very low energy interfaces. (2) The implied lattice parameters of stishovite for all of the orientation groups are good fits to the calculated lattice parameters for [001] kyanite and <110> spinel. Table A1 shows the angular relations of the orientation groups and their calculated and indexed directions assuming a stishovite host and compares the mismatch between the structures of the exsolved phases and stishovite. The misfits for the dominant orientation group (parallel to [001] of stishovite) are 4% for kyanite (2 unit cells of stishovite matched to 1 unit cell for kyanite) and 10% for ringwoodite/magnetite (4 unit cells of stishovite matched to 1 unit cell of spinel). The kyanite/stishovite fit is well within the range of misfits exhibited by known exsolution relationships and the spinel/stishovite fit improves to better than 2% for comparison of 9 unit cells of stishovite with 2 unit cells of spinel. The latter calculation shows that the most probable structure of these stishovite/spinel interfaces would have a misfit dislocation spaced every 9 stishovite unit cells apart to maintain the fit of the octahedral chains. Such semicoherent interfaces are common in precipitate/host relationships.

Had the pre-existing phase been coesite rather than stishovite, there would be no unique direction to assign to the most abundant set of needles and there would be no explanation for more than one mirror plane in the data. In particular, the set of 4 mirrors intersecting in the direction we identify as [001] stishovite would have to be due to coincidence, as would the mirror perpendicular to our chosen [001] stishovite direction. The facts that the orientation groups of precipitates exhibit (i) the tetragonal symmetry of stishovite and (ii) the same Miller Indices in the reconstructed stishovite crystals for all of the quartz domains analysed, place an extremely powerful constraint in this problem.

Appendix B. Evolution of exsolved spinel during exhumation

Eq. (1) of the main text describes exsolution of kyanite and spinel from stishovite. That simple equation would appear to fit the observations from the rock in question but it implicitly hypothesizes that hercynitic spinel is stable at pressure >9 GPa (which it is not) and that iron is entirely reduced upon exsolution. Known stability relations (Woodland and O'Neill, 1993; Woodland and Angel, 2000) provide a straightforward explanation for what spinel composition will exsolve under these conditions and how that composition will evolve during decompression.

The originally exsolving spinel in this system is a solid solution between Fe-rich ringwoodite, $(Mg, Fe)_2SiO_4$, and magnetite (Woodland and O'Neill, 1993; Woodland and Angel, 2000) — which modifies Eq. (1) to the following (ignoring the small Mg content for the time being):

$$\begin{aligned}(Si_{1-2x}Al^{3+}_{2x-a-b}Fe^{3+}_{a+b})O_{2-x} = {} & (1-3x+7b/4)SiO_2 \\ & +(x-a/2-b/2)Al_2SiO_5+(a/2-b/4) \\ & [Fe_{2+2b/(2a-b)}(Si_{1-4b/(2a-b)},Fe^{3+}_{4b/(2a-b)})O_4] \\ & +a/4O_2\end{aligned}$$

$$\mathrm{Al-Fe^{3+}-\ bearing\ stishovite} = \mathrm{stishovite+kyanite+Fe-ringwoodite/magnetite\ solid\ solution} \quad (1a)$$

where a and b are $Fe^{2+}$and Fe^{3+}, respectively ($b>>a$ in stishovite). Given that Fe^{3+} dissolves at least 10 times as much into stishovite as Fe^{2+}, the spinel composition can be expected to be dominated by magnetite (Woodland and O'Neill, 1993; Woodland and Angel, 2000). During decompression, the presence of a dominant magnetite component stabilizes the spinel to very low pressures; the ringwoodite-component progressively decreases to a few percent at less than 2 GPa (see Fig. 1 and Fig. 5 of Woodland and Angel (2000)), at which point the hercynite component begins to grow, with Al replacing both Si and Fe^{3+} (see Woodland and O'Neill, 1993: Table 1; Fig. 4 and Fig. 5). At ~1 GPa the spinel assumes the composition that is currently observed, yielding the right side of Eq. (1) (but including, of course, the Mg-component that has been eliminated from this discussion for simplicity). The final ratio of kyanite to hercynitic spinel will be fixed by the original Al/Fe ratio in stishovite and the small Mg content.

Is there any direct evidence for this scenario? Yes. Firstly, the hercynitic spinel in our sample participates in at least some, perhaps all, of the same orientation groups as kyanite, consistent with stishovite crystallography, strongly suggesting original exsolution of a spinel and compositional evolution during decompression. Secondly, the previously-determined pressure-dependence of composition of spinels in the $(Mg, Fe)_2SiO_4$–Fe_3O_4 system (Woodland and O'Neill, 1993; Woodland and Angel, 2000) illustrates how an originally exsolved magnetite/ringwoodite spinel would evolve during decompression to the composition observed in this rock at low pressure. Moreover, such evolution explains why in the rock under consideration hercynitic spinel of the composition [Fe/(Fe+Mg)=0.7–0.8] can coexist with kyanite (Fig. 4); had the originally precipitating Fe-bearing phase been garnet (the phase expected from bulk composition of the rock if the Fe were not oxidized), hercynitic spinel of the observed composition could form only in the sillimanite stability field (Bohlen et al., 1968).

Stishovite [001] was taken from Suito et al. (1996); their data were collected at P=10.5 GPa; data to T=800 °C were extrapolated to 1100 °C. Room temperature kyanite

[001] data of Comodi et al. (1997) were extrapolated from 5.8 GPa to 9.0 GPa and then extrapolated to 1100 °C using the thermal expansion data of Winter and Ghose (1979). Ringwoodite/magnetite solid solution data are those of experiment #uhp666 (9.3 GPa; 1100 °C) of Woodland and O'Neill (1993). Hercynitic spinel lattice parameters are close to those of magnetite, hence the evolution of lattice parameters during exhumation will have been dominated by expansion due to progressive loss of ringwoodite component during decompression.

Table A1
Orientations of precipitates and their fits to stishovite structure

Orientation groups and included angles		1	2	3	4	5	6	7
		Measured included angles (°)						
1	Calculated included angles (°)	–	70	67	86	95	135	137
2		68.9	–	136	147	155	140	81
3		68.9	137.9	–	28	35	77	135
4		84.5	149.9	30.1	–	10	52	108
5		95.5	149.9	37.2	10.9	–	43	100
6		138.6	134.9	80.4	56.4	45.9	–	61
7		138.6	80.4	134.9	106.2	97.9	55.7	–
Best fit in St structure		[001]	[503]	[$\bar{5}$03]	[$\bar{6}$31]	[$\bar{6}$3$\bar{1}$]	[$\bar{2}$2$\bar{5}$]	[22$\bar{5}$]
Axis length (a = 4.1625 Å)		2.6640 Å	22.2942	22.2942	28.0497	28.0497	17.7773	17.7773
[a]Fit	Ky [001] = 5.537 Å	3.9[b]	0.7	0.7	1.3	1.3	6.6	6.6
error	Ring/Mag 1:2	10.4[c]	5.6	5.6	4.9	4.9	0.7	0.7
(%)	<110> = 11.768 Å	1.8[d]	0.3	0.3	2.1	2.1	3.0	3.0

Note: St: stishovite; Ky: kyanite; Ring/Mag: $Ringwoodite_{0.36}Magnetite_{0.64}$.

[a]Misfits are within reasonable bounds based on other systems (see Appendix A text). Lattice parameter data for the three phases were calculated from experimental data as described in Appendix A text. St: 10.5 GPa, 1100 °C (Suito et al., 1996); Ky: 9.0 GPa, 1100 °C (Winter and Ghose, 1979; Comodi et al., 1997); Mag/Ring: 9.3 GPa; 1100 °C (Woodland and O'Neill, 1993).

[b]Kyanite: $(ky_{[001]} - 2st_{[001]})/2st_{[001]}$;

[c]$(ring/mag_{<110>} - 4st_{[001]})/4st_{[001]}$;

[d]$(2ring/mag_{<110>} - 9st_{[001]})/9st_{[001]}$. This calculation shows the fit to be excellent with 1 misfit dislocation/9 st unit cells (see Appendix A text).

Unshaded area shows measured angles between ppt groups; shaded area shows calculated angles assuming stishovite.

References

Bohlen, S.R., Dollase, W.A., Wall, V.J., 1968. Calibration and applications of spinel equilibria in the system $FeO–Al_2O_3–SiO_2$. J. Petrol. 27, 1143–1156.

Bozhilov, K.N., Green II, H.W., Dobrzhinetskaya, L.F., 1999. Clinoenstatite in Alpe Arami peridotite: additional evidence of very high pressure. Science 284, 128–132.

Bromily, G., Hilaret, N., McCammon, C., 2004. Solubility of hydrogen and ferric iron in rutile and TiO_2 (II): implications for phase assemblages during ultrahigh-pressure metamorphism and for the stability of silica polymorphs in the lower mantle. Geophys. Res. Lett. 31, L04610. doi:10.1029/2004GL019430.

Cahn, R.W., 1977. Physical Metallurgy, 2nd ed. North Holland, Amsterdam, pp. 1177–1180.

Chao, E.C.T., Fahey, J.J., Littler, J., Milton, D.J., 1962. Stishovite, a new mineral from Meteorite crater, Arizona. J. Geophys. Res. 67, 419–421.

Chopin, C., 1984. Coesite and pure pyrope in high-grade blue schists of the western Alps: a first record and some consequences. Contrib. Mineral. Petrol. 86, 107–118.

Chung, J.I., Kagi, H., 2002. High concentration of water in stishovite in the MORB system. Geophys. Res. Lett. 29, 2020. doi:10.1029/2002GL015579.

Comodi, P., Zanazzi, P.F., Poli, S., Schmidt, M.W., 1997. High-pressure behavior of kyanite: compressibility and structural deformations. Am. Mineral. 82, 452–459.

Dobrzhinetskaya, L.F., Green, H.W., Wang, S., 1996. Alpe Arami: a peridotite massif from depths of more than 300 km. Science 271, 1841–1846.

Dobrzhinetskaya, L.F., Green II, H.W., Renfro, A.P., Bozhilov, K.N., Spengler, D., Van Roermund, H.L.M., 2004. Precipitation of pyroxenes and Mg_2SiO_4 from majoritic garnet: simulation of peridotite exhumation from great depth. Terra Nova 16, 325–330.

El Goresy, A., Dubrovinsky, L., Sharp, T.G., Saxena, S.K., Chen, M., 2000. A monoclinic post-stishovite polymorph of silica in the Shergotty Meteorite. Science 288, 1632–1634.

Green, H.W., Dobrzhinetskaya, L., Bozhilov, K.N., 2000. Mineralogical and experimental evidence for very deep exhumation from subduction zones. J. Geodyn. 30, 61–76.

Holland, T.J.B., Powell, R., 1998. An internally consistent thermodynamic data set for phases of petrological interest. J. Metamorph. Geol. 16, 309–343.

Irifune, T., Ringwood, A.E., 1993. Phase transformations in subducted oceanic crust and buoyancy relationships at depths of 600–800 km in the mantle. Earth Planet. Sci. Lett. 117, 101–110.

Irifune, T., Ringwood, A.E., Hibberson, W.O., 1994. Subduction of continental crust and terrigenous and pelagic sediments: an experimental study. Earth Planet. Sci. Lett. 126, 351–368.

Landtwing, M.R., Pettke, T., 2005. Relationships between SEM-cathdoluminescence response and trace-element composition of hydrothermal vein quartz. Am. Mineral. 90, 122–131.

Liu, L., Chen, D.L., Zhang, A.D., Sun, Y., Wang, Y., Yang, J.X., Luo, J.H., 2005. Ultrahigh pressure(>7 GPa) gneissic K-feldspar (-bearing) garnet clinopyroxene in the Altyn Tagh, NW China: evidence from clinopyroxene exsolution in garnet. Sci. China (D) 48 (7), 1000–1010.

Liu, X., Jin, Z., Green II, H.W., 2007. Clinoenstatite exsolution in diopsidic augite of Dabieshan: Garnet peridotite from depth of 300 km. Am. Mineral. 92, 546–552.

Ogasawara, Y., Fukasawa, K., Maruyama, S., 2002. Coesite exsolution from supersilicic titanite in UHP marble form the Kokchetav Massif, northern Kazakhstan. Am. Mineral. 87, 454–461.

Ono, S., 1998. Stability limits of hydrous minerals in sediment and mid-ocean ridge basalt compositions: implications for water transport in subduction zones. J. Geophys. Res. 103, 18253–18267.

Ono, S., 1999. High temperature stability limit of phase egg, $AlSiO_3$ (OH). Contrib. Mineral. Petrol. 137, 83–89.

Pawley, A.R., McMillan, P.F., Holloway, J.R., 1993. Hydrogen in stishovite, with implications for mantle water content. Science 261, 1024–1026.

Sharp, T.G., El Goresy, A., Wopenka, B., Chen, M., 1999. A post-stishovite SiO_2 polymorph in the Meteorite Shergotty: implications for impact events. Science 284, 1511–1513.

Smith, D.C., 1984. Coesite in clinopyroxene in the Caledonides and its implications for geodynamics. Nature 310, 641–644.

Smyth, J.R., Hatton, C.J., 1977. A coesite–sanidine grospydite from the Roberts Victor kimberlite. Earth Planet. Sci. Lett. 34, 284–290.

Sobolev, N.V., Shatsky, V.S., 1990. Diamond inclusions in garnets from metamorphic rocks. Nature 343, 742–756.

Sobolev, A.V., Hofmann, A.W., Sobolev, S.V., Nikogosian, I.K., 2005. An olivine-free mantle source of Hawaiian shield basalts. Nature 434, 590–597.

Suito, K., Miyoshi, M., Onodera, A., Shimomura, O., Kikegawa, T., 1996. Thermal expansion studies of stishovite at 10.5 GPa using synchrotron radiation. Phys. Earth Planet. Inter. 93, 215–222.

Van der Hilst, R., Widiyanyoro, S., Engdahl, E.R., 1997. Evidence for deep mantle circulation from global tomography. Nature 386, 578–584.

Van Roermund, H.L.M., Drury, M.R., 1998. Ultra-high-pressure (P>6 GPa) garnet peridotites in Western Norway: exhumation of mantle rocks from >185 km depth. Terra Nova 10, 295–302.

Winter, K., Ghose, S., 1979. Thermal expansion and high-temperature crystal chemistry of the Al_2SiO_5 polymorphs. Am. Mineral. 64, 573–586.

Wirth, R., Kaminsky, F., Matsyuk, S., Kaminsky, F., 2007. Inclusions of nanocrystalline hydrous aluminium silicate "Phase Egg" in superdeep diamonds from Juina (Mato Grosso State, Brazil). Earth Planet. Sci. Lett. 259, 384–399.

Woodland, A.B., Angel, R.J., 2000. Phase relations in the system fayalite–magnetite at high pressures and temperatures. Contrib. Mineral. Petrol. 139, 734–747.

Woodland, A.B., O'Neill, H.S.C., 1993. Synthesis and stability of $Fe^2{}_3+Fe^3{}_2+Si_3O_{12}$ garnet and phase relations with $Fe_3Al_2Si_3O_{12}$–$Fe^2{}_3+Fe^3{}_2+Si_3O_{12}$ solutions. Am. Mineral. 78, 1002–1015.

Ye, K., Cong, B.L., Ye, D.N., 2000. The possible subduction of continental material to depths greater than 200 km. Nature 407, 734–736.

Yang, J.S., Xu, Z.Q., Zhang, J.X., Song, S.G., Wu, C.L., Shi, R.D., Li, H.B., Maurice, B., 2002. Early Palaeozoic north Qaidam UHP metamorphic belt on the north-eastern Tibetan plateau and a paired subduction model. Terra Nova 14 (5), 397–404.

Zhang, L.F., Song, S.G., Liou, J.G., Ai, Y.L., Li, X.P., 2005. Relict coesite exsolution in omphacite from Western Tianshan eclogites, China. Am. Mineral. 90, 181–186.